DOI: 10.1002/elan.201500171

Acidic and Basic Functionalized Carbon Nanomaterials as Electrical Bridges in Enzyme Loaded Chitosan/Poly(styrene sulfonate) Self-Assembled Layer-by-Layer Glucose Biosensors

Melinda David,[a, b] Madalina M. Barsan,[a] Monica Florescu,[b] and Christopher M. A. Brett*[a]

Abstract: Glucose oxidase (GOx) was incorporated in a self-assembled multilayer modified gold electrode, based on electrostatic interaction between positively charged chitosan polymer, containing GOx, and negatively charged poly(styrene sulfonate). Good electronic communication between electrode and enzyme was ensured by carbon nanomaterials (CN), graphene (G) or carbon nanotubes (CNT) functionalised in either HNO_3 or KOH, immobilized together with the enzyme. Cyclic voltammetry and electrochemical impedance spectroscopy enabled identification of the glucose biosensor assemblies with the best functionalized CN, KOH_G and HNO_3_CNT, confirmed by fixed potential amperometry at −0.3 V vs. Ag/AgCl, these glucose biosensors exhibiting the highest sensitivities and lowest detection limits.

Keywords: Layer-by-layer · Self-assembly · Functionalized graphene · Functionalized carbon nanotubes · Glucose biosensors

1 Introduction

Electrochemical enzyme-based biosensors are uniquely efficient in translating biochemical events [1]. The immobilization of the enzyme is an important factor in the performance of the biosensor [2], and immobilization based on self-assembled mono- or multilayers enables the formation of uniform and stable structures [3]. Self-assembly occurs via physical immobilization [4], by weak bonds such as Van der Waal's forces and electrostatic and/or hydrophobic interactions, therefore not destroying enzymatic activity and suitable for the reproducible immobilization of enzymes, with good preservation of activity [5]; in such configurations, direct electron transfer between enzyme and electrode is possible [6,7]. Layer-by-layer deposition uses a variety of polyelectrolytes alternating with oppositely charged enzyme layers. Some of the predominantly used polycations are poly(ethyleneimine) PEI [8,9], poly(dimethyldiallylammonium chloride) PDDA [10], or chitosan or its derivatives [11–13]; the most commonly used polyanions are poly(styrene sulfonate) PSS^- [14], poly(acrylic acid) PAA and poly(vinyl sulfonate) PVS^- [15].

In previous work, we developed a strategy for new biosensor architectures based on multilayer films containing glucose oxidase (GOx) together with nitrogen-doped graphene (NG) dispersed in the biocompatible positively-charged polymer chitosan ($chit^+$(NG + GOx)), together with the negatively charged polymer poly(styrene sulfonate), PSS^- [16]. PSS^- was chosen as the polyanion, due to its easy binding to any other oppositely-charged molecules [17] and chitosan, as a polycation, provides a good adsorption matrix with high mechanical stability and high affinity to proteins, biocompatibility and non-toxicity [7,18–20].

In the present study, graphene (G) and carbon nanotubes (CNT) were functionalized in acidic or basic media in order to ascertain which of the four materials is best for use in LbL multilayer biosensors. The use of both of these carbon nanomaterials (CN) as electrocatalysts in biochemical devices is widely known [21–23], functionalization being crucial for efficient action. Surface functionalization increases the specific capacitance of CN, and introduces functional groups or heteroatoms responsible for the increasing the hydrophilicity of the carbon materials, thus enabling rapid electrolyte ion transport [24]. Acidic treatment introduces functional groups, while treatment with strong bases introduces heteroatoms into the lattice, leading to a nanoporous material [25–28]. Four different LbL architectures were constructed on Au electrode substrates, incorporating one of the four forms of functionalised CN, together with glucose oxidase (GOx) as model enzyme to form Au/{$chit^+$(CN + GOx)/PSS^-}$_n$. The biosensors were electrochemically characterized after each bilayer deposition, and their analytical properties were

[a] M. David, M. M. Barsan, C. M. A. Brett
Department of Chemistry, Faculty of Sciences and Technology, University of Coimbra
3004–535 Coimbra, Portugal
tel: +351-239854470; fax: +351-239827703
*e-mail: cbrett@ci.uc.pt

[b] M. David, M. Florescu
Facultatea de Medicina, Universitatea Transilvania din Brasov
Brasov 500019, Romania

determined and compared, in order to choose the best biosensor architecture.

2 Experimental

2.1 Materials

Glucose, ascorbic acid, catechol, citric acid, dopamine, fructose, oxalic acid, uric acid potassium hydroxide, polystyrene sulfonate (PSS^-) and chitosan (low molecular weight, minimum 85% degree of deacetylation) were purchased from Sigma-Aldrich. CNT were from Nanolab, University of Western Ontario, Canada and GOx extracted from *Aspergillus niger* (24 U/mg) was purchased from Fluka. Graphene was a kind gift from Prof. X. Sun, and it was obtained from graphite oxide by heating at 1050 °C for 30 s under Ar [29].

The aqueous glucose solution was prepared 24 h prior to measurements, in order to obtain the biologically active form (α-D-glucose).

The buffer solution used for all experiments contained a mixture of monosodium phosphate, (NaH_2PO_4) and disodium phosphate, (Na_2HPO_4) 0.1 M, pH 7.0 (from Sigma-Aldrich).

Millipore Milli-Q nanopure water and analytical reagents were used for the preparation of all solutions. All experiments were performed at room temperature (~25 °C) and all biosensors were kept in buffer solution at ~4 °C when not in use.

2.2 Instruments

All electrochemical measurements were carried out in a conventional electrochemical cell containing three electrodes: a bulk gold disc electrode (area 0.00785 cm^2) or a Au quartz crystal disc (AuQC) (exposed area 0.205 cm^2), as working electrode, a platinum foil as counter electrode and a saturated Ag/AgCl electrode as reference. Chrono-amperometric and voltammetric measurements were performed by using a computer-controlled μ-Autolab Type II potentiostat-galvanostat running with GPES (general purpose electrochemical system) version 4.9 software (Metrohm-Autolab, Utrecht, Netherlands).

Scanning electron microscopy (SEM) images were taken with a Merlin Scanning Electron Microscope with Gemini 2 column, Carl Zeiss, Germany, using an accelerating voltage of 2 kV. For the SEM analysis, indium tin oxide electrodes were used as substrates for the deposition of the nanomaterials.

Gravimetric measurements were performed with an electrochemical quartz crystal microbalance (EQCM), model eQCM 10 M (Gamry Instruments, USA), containing an Au quartz crystal (AuQC) with 10 MHz central frequency.

Electrochemical impedance measurements were done with a Reference 600 potentiostat/galvanostat/ZRA (Gamry Instruments, USA). A frequency range of 65 kHz – 0.1 Hz was used, by applying a rms perturbation of 10 mV, with 10 frequency values per frequency decade, at an applied potential of 0.0 V vs. Ag/AgCl.

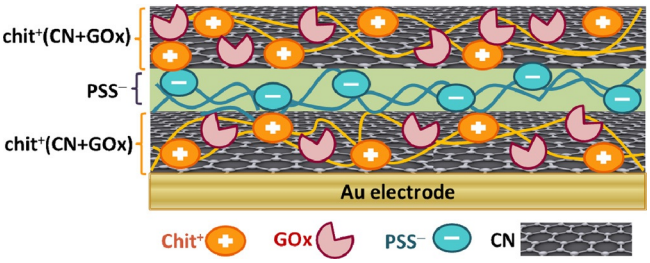

Scheme 1. LbL assembly on the gold surface showing sequential layers of $\{chit^+(CN+GOx)/PSS^-\}_n$.

2.3 Fabrication of the LbL Glucose Biosensor

The Au bulk disc electrode was cleaned by cyclic scanning in a 0.1 M sulfuric acid solution in the potential range from −0.5 V to 1.5 V at a scan rate of 100 $mV\,s^{-1}$. The AuQC surface was carefully cleaned with acetone.

Basic functionalization of G and CNT was carried out with 7.0 M KOH, by stirring the G/CNT dispersion for 2 h followed by 12 h without stirring. Acidic functionalization was done in 3 M nitric acid by stirring the G/CNT dispersion for approximately 12 h. All four types of functionalized G/CNT were washed until neutral pH and dried overnight at 60 °C. Following this, chitosan suspensions were formed, by mixing them with chitosan solution (0.5 or 1% w/v chitosan in 1% v/v acetic acid) and sonicating for 3 h, for a better dispersion, before adding the enzyme, to obtain a 0.5, 1.0 or 2.0% GOx and 0.05% functionalized CN chitosan loaded solution, denoted as $chit^+(CN+GOx)$.

The clean electrodes were modified step-by-step using the self-assembly LbL procedure, first being immersed in $chit^+(CN+GOx)$, for 1 h, washed with Milli-Q water to remove residual molecules and dried under a stream of N_2. Next, the electrodes were immersed in PSS^- solution (1% dissolved in water), for 20 min, washed and dried [16]. The above steps were repeated until the desired number of layers was reached, up to a maximum of 4 bilayers. A schematic representation of the electrode modification is presented in Scheme 1.

3 Results and Discussion

3.1 SEM Characterization of Nanomaterials

SEM examination of all four types of nanomaterials dispersed in chitosan provides an overview of their nanostructures. Typical SEM images of the graphene, both acidic and basic functionalized, are shown in Figure 1A, B and reveal the morphology of the graphene sheets, with wrinkled structure. The sheets are randomly crumpled and form a rather disordered material. The graphene planar sheets are clearly observed in the magnified figure

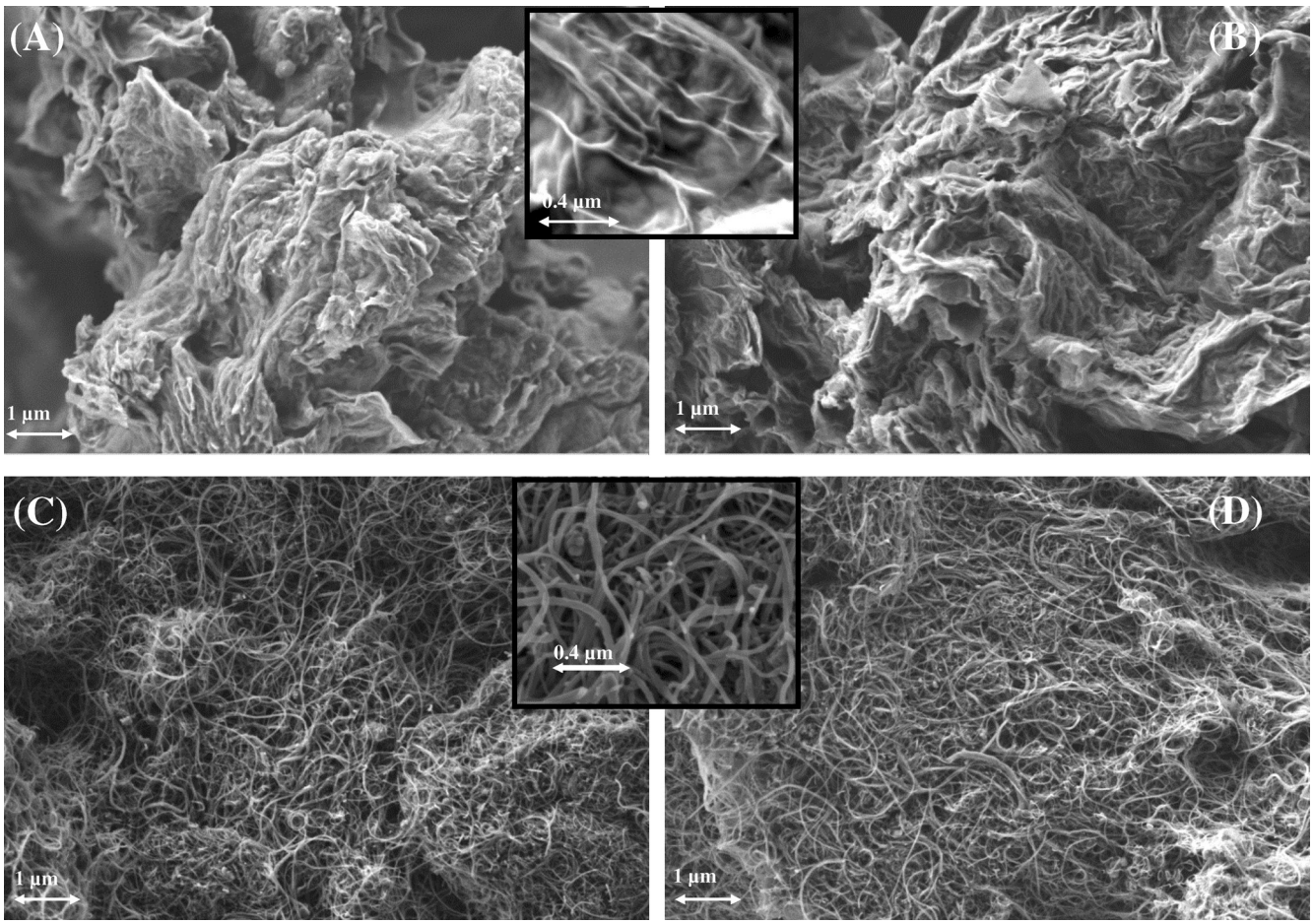

Fig. 1. SEM images of A) HNO_3_G, B), KOH_G, C) HNO_3_CNT and D) KOH_CNT.

and, indicate that the two-dimensional structure of graphene [29] is well maintained after their functionalization. However, it is hard to distinguish the difference between acidic and basic functionalized graphene.

Typical SEM images of MWCNT are displayed in Figure 1C and D and clearly reveal the tubular structure of the CNT in the typical non-aligned arrangement of CNT. There is no sign of residual metal particles. The nanotubes have diameters between 20 and 44 nm, which corresponds with the values declared by the producer (30 ± 10 nm), and indicates that their functionalization does not modify their initial structure. Also, in this case, they are no visible differences between the acidic and basic functionalized CNT.

3.2 Biosensor Fabrication and Optimization

In order to determine the most effective G/CNT containing layer-by-layer deposited film, the concentration of enzyme and chitosan was varied, and the electrochemical properties and sensitivities of the obtained biosensors were evaluated. For these optimization measurements acid-functionalised CNT, HNO_3_CNT, was used in the biosensor preparation.

First, the concentration of the enzyme solution was varied, from 0.5% up to 2.0%, in 1.0% chitosan solution, previously used in [16]. The modification of Au electrodes was done by 4 bilayers. The lowest sensitivity of 7.6 $\mu A\,cm^{-2}\,mM^{-1}$ was obtained for the biosensor containing 2.0% GOx, which also lost 25% of its sensitivity after one week. For a concentration of 0.5% GOx, the sensitivity was 9.3 $\mu A\,cm^{-2}\,mM^{-1}$, and for 1.0%, 13.4 $\mu A\,cm^{-2}\,mM^{-1}$. The fact that the enzyme concentration of 2.0% was too high suggests that the agglomeration of enzyme molecules leads to a small number of available binding sites. It was observed that for 0.5% enzyme concentration, the biosensor sensitivity started to decrease after the first week (23% lost), remaining almost constant for the 1.0% one, which also had a higher initial sensitivity. These results led to the choice of an enzyme concentration of 1.0% GOx in construction of the biosensor platform.

Since it is known that the chitosan concentration as well as its molecular weight and degree of deacetylation play a very important role in enzyme immobilization [30], two chitosan concentrations of 0.5 and 1.0% were tested. Decreasing the concentration from 1.0 to 0.5%, resulted in an increase in biosensor sensitivity from 13.4 $\mu A\,cm^{-2}\,mM^{-1}$ to 18.6 $\mu A\,cm^{-2}\,mM^{-1}$. This is due to

an increase in chitosan film conductivity, observed in the electrochemical impedance spectra by a decrease in the total impedance value, and in the CVs by an increase in the capacitive currents (results not shown). Taking this into account, the optimum composition of enzymatic layer contained 0.5% of chitosan and 1.0% of GOx enzyme, which was used in further studies.

Unfunctionalized graphene and CNT were also assayed as control nanomaterials. Untreated graphene and untreated CNT are both highly hydrophobic and do not form uniform dispersions in the chitosan solution; hence, they are washed out between layer deposition thus explaining the performance of these two biosensors being very similar to that of the biosensor not containing any carbon nanomaterial.

The effect of applied potential on the performance of biosensors based on all four types of nanomaterial was also studied for potentials between −0.4 and 0.0 V vs. Ag/AgCl. The biosensor sensitivities varied similarly for all 4 types of nanomaterials, exhibiting highest sensitivities at −0.4 V vs. Ag/AgCl and decreasing with less negative potential; the biosensors stopped working at potentials more positive than −0.15 V vs. Ag/AgCl. This tendency was already observed for other unmediated biosensors based on carbon nanomaterials, and can be explained taking into account the enzymatic mechanism based on regeneration of the enzyme cofactor at the carbon nanomaterial, which occurs at around −0.4 V [31,32]. Since at −0.3 V vs. Ag/AgCl the sensitivity was ~80% of that at −0.4 V, while at −0.2 V it decreased to 60%, in order to avoid too negative a potential, −0.3 V was chosen for further measurements.

3.3 Gravimetric Monitoring of the LbL Deposition

The EQCM was used to monitor the adsorption process during LbL self-assembly of chit$^+$(CN+GOx) and PSS$^-$ monolayers, using a 1% chit solution. Considering that the monolayers were rigid films, the deposited mass was determined using the Sauerbrey equation [33]:

$$\Delta f = -\frac{2f_0^2}{A\sqrt{\mu_q \rho_q}}\Delta m \quad (1)$$

where f_0 is the resonant frequency (Hz), Δf the frequency change (Hz), Δm the mass change (g), A the piezoelectrically active crystal area, ρ_q the density of quartz (g cm^{-3}) and μ_q the shear modulus of quartz for AT-cut crystals (g cm^{-1} s^{-2}). The AuQC employed in this study has a conversion factor, $-\Delta f/\Delta m$, of 226.0 Hz per 1 μg.

An example of a gravimetric measurement for HNO_3_CNT is shown in Figure 2, which displays the frequency changes recorded during the LbL deposition on AuQC. In the first step in the LbL deposition, i.e. AuQC immersion in chit$^+$(CN+GOx) solution, the frequency hardly changed, indicating insignificant adsorption. Immersion in PSS$^-$ solution led to a 3.0 kHz frequency change, corresponding to 2.8 μg of PSS$^-$ deposited. During the second

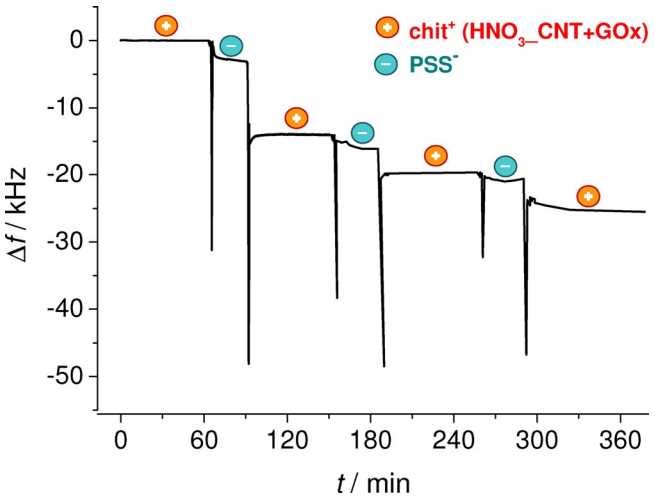

Fig. 2. Frequency shift during the LbL assembly of AuQC/{chit$^+$(HNO_3_CNT+GOx)/PSS$^-$}$_n$, n=1–4.

immersion of the crystal in chit$^+$(CN+GOx) solution, the frequency shifted significantly, the total amount adsorbed being 10 μg. The second and third PSS$^-$ layers were thinner than the first one, 2.0 and 1.0 μg respectively. Similarly, the third and fourth chit$^+$(CN+GOx) layers were thinner than the second one, being 3.5 and 4.1 μg, respectively.

The total decrease in frequency was Δf_{tot}=25.2 kHz, corresponding to a deposited film of m_{tot}=23.4 μg.

3.4 Electrochemical Characterization of the Biosensors

3.4.1 Cyclic Voltammetry

Cyclic voltammograms (CV) were recorded for the different electrode architectures after each bilayer modification, up to 4 bilayers. Measurements were done in 0.1 M NaPB pH 7.0 at a scan rate of 50 mV s^{-1}. Figure 3 shows CVs of the bare electrode, and the electrodes modified with 1, 2, 3 and 4 chit$^+$/PSS$^-$ bilayers in the presence of the four CN. The PSS$^-$ layer did not change the CV profile, only having the role of charge conduction. The capacitance values were calculated at a fixed potential of 0.1 V, except for the HNO_3_CNT biosensor which was 0.3 V in order to avoid the redox reaction region, and the results are shown in Table 1.

As observed, the capacitance calculated for the bare AuQC electrode increases substantially with modification. For both types of functionalized CNT, the tendency of the capacitance is to grow with each chit$^+$(CNT+GOx)/PSS$^-$ bilayer, the values calculated for the first bilayer being very similar. The highest capacitance value was calculated for HNO_3_CNT, as shown in the Table 1, being 1070 μF cm^{-2} for the 4th bilayer, while the AuQC/{chit$^+$(KOH_CNT+GOx)//PSS$^-$}$_4$ gave only 600 μF cm^{-2} for the 4th bilayer. Beside the capacitive currents, the AuQC/{chit$^+$(HNO_3_CNT+GOx)/PSS$^-$}$_n$ modified electrode also showed faradaic currents (see Figure 3C), the redox

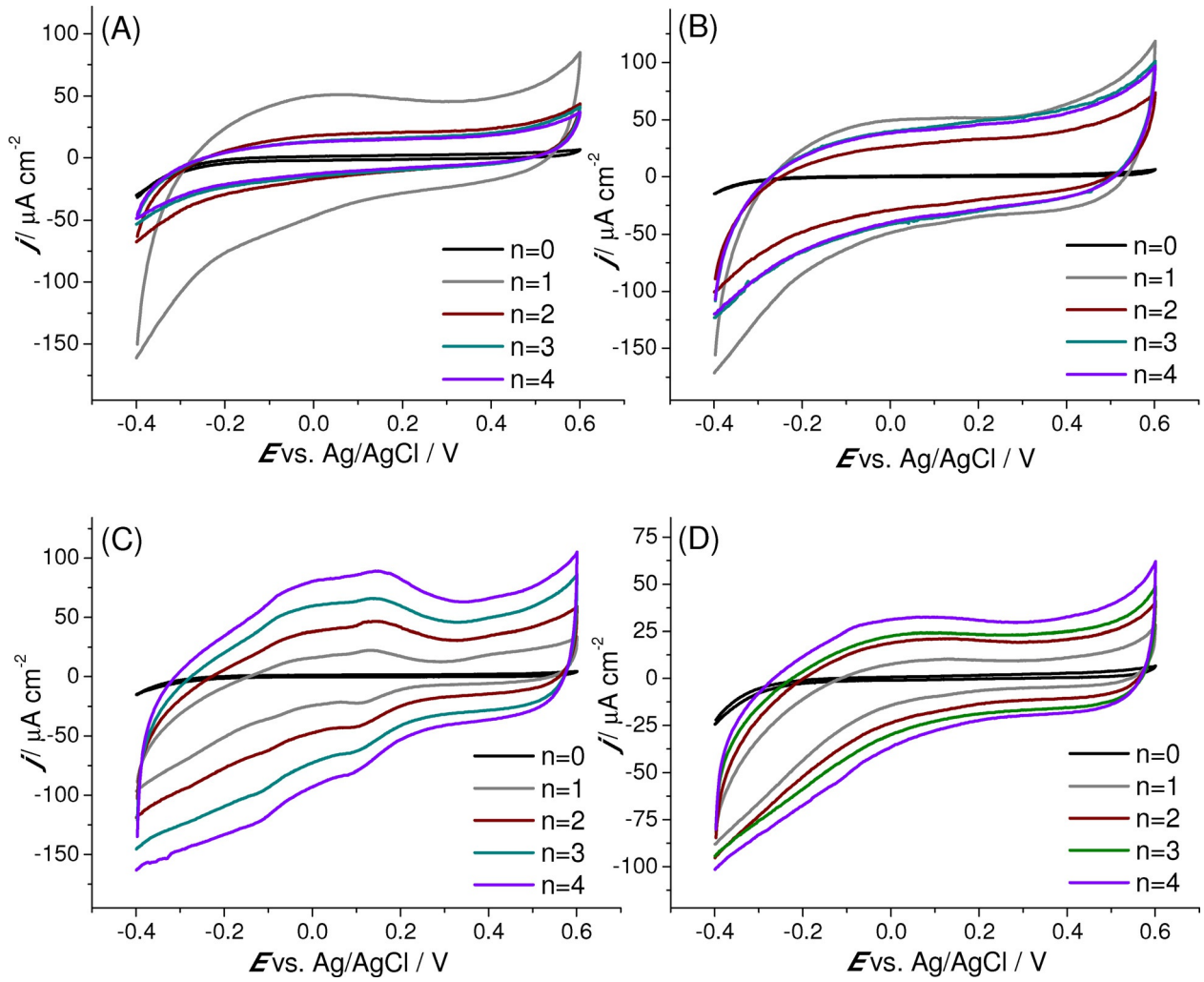

Fig. 3. CVs recorded in 0.1 M NaPB pH 7.0 at AuQC/{chit$^+$(CN + GOx)/PSS$^-$}$_n$, n = 0–4, where CN are A) HNO_3_G, B) KOH_G, C) HNO_3_CNT and D) KOH_CNT; v = 50 mV s^{-1}.

Table 1. Capacitance values calculated for AuQC/{chit$^+$(CN + GOx)/PSS$^-$}$_n$ from the cyclic voltammograms in Figure 3.

CN	C (µF cm^{-2})			
	HNO_3_G	KOH_G	HNO_3_CNT	KOH_CNT
n = 0	40	40	40	40
n = 1	850	950	210	200
n = 2	350	550	490	390
n = 3	280	810	780	470
n = 4	280	810	1070	600

peaks being characteristic for the reversible oxidation of oxygen-containing functional groups [34].

In the case of LbL modification with functionalized graphene (see Figure 3A and B), the modified electrode with highest capacitance value was for one bilayer, with very similar values of 850 and 950 µF cm^{-2} for HNO_3_G and KOH_G, respectively. The modifications with further bilayers had different effects on the capacitive current. It decreased for both electrodes in the 2 bilayer configuration, but while further deposition of HNO_3_G containing layers lead to a decrease in the C value, to 280 µF cm^{-2}, for n = 3 and 4; the contrary was observed in the case of KOH_G modified electrodes, which had higher C values for n = 3 and 4, of 810 µF cm^{-2}. This clearly indicates that KOH functionalization works better than the acidic treatment in the case of graphene. The acidic treatment did not confer so much hydrophilicity to the material, so that, due to agglomerate formation, the deposition of multiple bilayers did not further increase the capacitance of the electrode modified compared with only one bilayer.

In the absence of CN in the chitosan layer, the capacitance of the Au electrode decreases linearly from 40 µF cm^{-2} for the bare AuQC to 34, 28, 20 and 13 µF cm^{-2} for the electrodes modified with 1, 2, 3 and 4 bilayers, respectively. This is explained by the relatively poor conductivity of the chitosan polymer [35], which is significantly improved by the dispersion of either functionalized G or CNT.

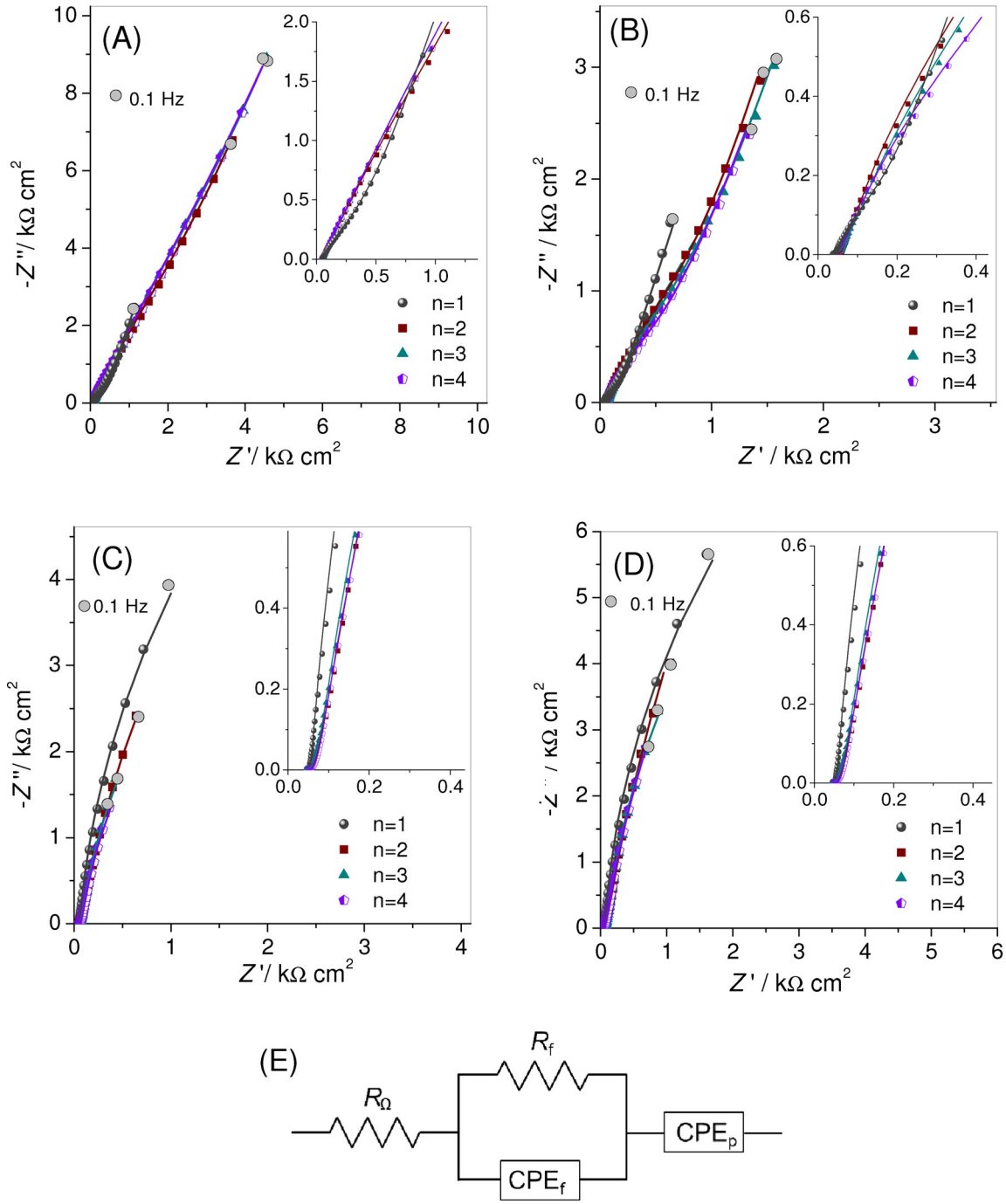

Fig. 4. Impedance spectra recorded in 0.1 M NaPB pH 7.0 at AuQC/{chit$^+$(CN + GOx)/PSS$^-$}$_n$, n = 1–4, where CN are A) HNO_3_G, B) KOH_G, C) HNO_3_CNT and D) KOH_CNT; E) the equivalent circuit used to fit the spectra; applied potential 0.0 V vs. Ag/AgCl.

3.4.2 Electrochemical Impedance Characterization

Electrochemical impedance spectroscopy was employed to analyse the surface and bulk characteristics of the AuQC/{chit$^+$(CN + GOx)/PSS$^-$}$_n$. Complex plane spectra are presented in Figures 4A–D. The modification of the electrodes with any of the LbL configurations leads to a significant decrease in the impedance values at 0.1 Hz, by a factor of ~1000, compared to the bare AuQC (results not shown). This decrease in impedance values was more significant than what was observed in a similar LbL architecture, in which enzyme and nitrogen-doped graphene were entrapped in 1.0% w/v chitosan solution [16], due to the use of a less concentrated chitosan solution of 0.5% in the present study. In the absence of CN in the chitosan layer, the impedance at 0.1 Hz increases gradually with each bilayer deposition, in agreement with the results obtained by cyclic voltammetry.

Table 2. Electrical equivalent circuit element values obtained by fitting the impedance spectra in Figure 4 for AuQC/{chit$^+$(CN+GOx)/PSS$^-$}$_n$, n=1–4.

	n	R_f (kΩ cm^2)		CPE_f (μF cm^{-2} s$^{\alpha-1}$)		α_1		CPE_p (μF cm^{-2} s$^{\alpha-1}$)		α_2	
		HNO_3	KOH	HNO_3	KOH	HNO_3	KOH	HNO_3	KOH	HNO_3	KOH
Graphene	1	0.2	0.1	700	1090	0.79	0.87	1040	1070	0.70	0.80
	2	5.1	0.6	310	762	0.67	0.85	340	605	0.88	0.82
	3	6.3	0.6	302	762	0.65	0.83	251	560	0.85	0.80
	4	6.5	0.3	260	845	0.88	0.87	263	682	0.88	0.78
CNT	1	24.2	32.5	465	321	0.96	0.94				
	2	24.0	56.6	763	461	0.92	0.91				
	3	12.8	21.0	1130	580	0.96	0.96				
	4	12.3	23.9	1376	683	0.94	0.94				

The spectra were fitted to the electrical equivalent circuit shown in Figure 4E. This consists in a cell resistance, R_Ω, in series with a parallel RC combination of a film resistance, R_f, and a film pseudocapacitance (CPE_f), represented as a constant phase element. The CPE are modelled as non-ideal capacitors, described by $CPE = -(i\ \omega\ C)^{-\alpha}$, where ω is the angular frequency and the α exponent reflects a non-uniform surface, and has values between 1.0 for a completely smooth and uniform surface and 0.5 for a porous electrode [36]. This RCPE combination was used to fit the intermediate frequencies at graphene modified electrodes and intermediate and low frequency regions at CNT-modified electrodes. Impedance in the high and middle frequency range senses the processes at the interface between the electrode and the first chit$^+$(CN+GOx) layer as well as the contacts between CN particles, while the capacitive behaviour of the upper chit$^+$(CN+GOx) contacting with the electrolyte is seen in the low frequency region for incorporated graphene, described by CPE_p.

At high frequencies, all spectra presented a very depressed semicircle that, in most cases, becomes a horizontal line parallel to the real axis. This behaviour is similar to that of supercapacitors, which at very high frequencies behave like pure resistors, and can be attributed to the lack of ion penetration into the micropores of the graphene or CNT layer [24]. This part of the spectra was neglected during the fittings, and the resistance values estimated from the complex plane plots were very low and similar for all the LbL modified electrodes in different configuration, being between 5 and 9 Ω cm^2. For comparison, the spectra recorded at bare AuQC presented a semicircle, fitted by an RCPE combination of charge transfer resistance of 492 kΩ cm^2 and a double layer pseudo-capacitance of 9.3 μF cm^{-2} s$^{\alpha-1}$ (α=0.93).

The values of the equivalent circuit elements are presented in Table 2. It can be seen that the film resistance R_f was smaller at G- than at CNT-modified electrodes. Since R_f comprises both the resistance between the carbon material and the electrode and that between the carbon nanomaterials, the smaller values for graphene can be explained by its better dispersion in the chitosan layer, graphene sheets being smaller than CNT, the latter forming a chit film with longer gaps between the conducting nanoparticles, which leads to an increase in the overall film resistance. Moreover, possibly more oxygen-containing functional groups are formed at CNT, due to defects on the side walls, which also can contribute to the observed increase in R_f, due to an increase in the contact resistance at the electrode/chit$^+$(CNT+GOx) interface [35]. For graphene, basic functionalization lead to a less resistive film, while in the case of CNT, the acidic treatment is better, also reflected by the higher CPE_f values of KOH_G and HNO_3_CNT compared to HNO_3_G and KOH_CNT. It can be seen that multilayer-modified electrodes incorporating CNT have higher values of the α exponent of CPE_f, that can possibly be due to a higher degree of nanoscale smoothness. The capacitance of the modified electrodes depends mainly on the surface area accessible to the electrolyte ions, which depends in turn on the specific surface area, pore-size distribution and shape, HNO_3_CNT and KOH_G modification allowing better ion penetration.

At CNT treated with acid, there is a faradaic reaction at 0.0 V, related to redox reactions of oxygen-containing functional groups, as also seen in the CV (see Figure 3C), which adds an extra faradaic capacitance and a charge transfer resistance [34,37]. For 2 bilayers, the R_f values were 0.6 and 5.1 for G, while for CNT they were 56.6 and 24.0 kΩ cm^2, for KOH and HNO_3 treated material, respectively. For the same 2 bilayers, the CPE_f values were very similar for KOH_G and HNO_3_CNT, 760 μF cm^{-2} s$^{\alpha-1}$, and for HNO_3_G and KOH_CNT, 310 and 461 μF cm^{-2} s$^{\alpha-1}$. The R_f values have a tendency to increase from 1 to 2 bilayers, decreasing for the third and fourth bilayers. The value of CPE_f increases with the number of bilayers in the case of CNT, while for G, the highest CPE_f was recorded for the first layer. The same variation profile was observed by cyclic voltammetry, in the capacitance values in Table 1, which were very similar to the CPE_f values obtained by the equivalent circuit fitting of the spectra.

The CPE_p capacitance of the graphene-modified electrodes showed the same tendencies as CPE_f, being the highest for the first bilayer deposited, ~1 mF cm^{-2} s$^{\alpha-1}$ for both basic and acid-treated G. This capacitance is attributed to charge separation inside the pores of the material, which will be influenced by the penetration of ions inside

the pores. The pore size and their distribution are the key factors for this type of pseudo-capacitance [38], and the fact that the CNT-containing layer did not exhibit this capacitive behaviour in the low frequency region is probably due to the larger pore size and their more uneven distribution within the chitosan film, since it is known that such factors lead to a significant decrease of the capacitance. The deposition of a second bilayer leads to a decrease by one half and a third for the KOH_G and HNO_3_G, respectively. While in the former case, the CPE_p values remains approximately the same for the third and fourth bilayer deposition, in the latter case the value continues to decrease up to the last deposition layer, indicating again that better functionalization of G for sensor purposes was achieved by using KOH.

3.5 Glucose Detection

3.5.1 Analytical Parameters of AuQC/ chit$^+$(GOx)$_n$/ (PSS$^-$)$_{n-1}$ Biosensors

To investigate the analytical performance of Au/{chit$^+$(CN + GOx)/PSS$^-$}$_n$ biosensors, fixed potential amperometry was performed at −0.3 V vs. Ag/AgCl in 0.1 M NaPB pH 7.0 with the addition of aliquots of glucose solution, the increase in current upon glucose addition being measured. A typical current vs. time trace is shown in Figure 5 for a Au/{chit$^+$(KOH_CNT + GOx)/PSS$^-$}$_4$ modified electrode, together with the corresponding calibration plot. All biosensors containing 4 bilayers had a similar linear range between 0.2 and 1.6 mM, with the sensitivities and detection limits shown in Table 3.

As expected from the electrochemical characterization, the biosensors containing KOH_G and HNO_3_CNT had the best and very similar analytical performances, with sensitivities of 18.6 μA cm^{-2} mM^{-1}, and detection limits of 12 and 18 μM, the lowest being for that incorporating KOH_G. The biosensor with lowest sensitivity, of 6.0 μA cm^{-2} mM^{-1} was that with HNO_3_G, which also had the highest detection limit, 64 μM, while that with KOH_G had a sensitivity of 13.7 μA cm^{-2} mM^{-1}, and 50 μM detection limit. The sensitivities followed the same trend as the capacitance and CPE_f variation observed in the CV and EIS measurements, the biosensors with highest sensitivities being those that had highest capacitances, with HNO_3_CNT and KOH_G, followed by that containing KOH_CNT and lastly HNO_3_G.

The sensitivity of the sensors was also tested after each bilayer deposition, for Au/{chit$^+$(CN + GOx)/PSS$^-$}$_n$, n = 1–4. Biosensors containing KOH_ and HNO_3_CNT showed a linear increase in sensitivity with each bilayer deposition, doubling in value from 2 to 4 bilayers, from 9.0 to 18.6 μA cm^{-2} mM^{-1}. For biosensors with HNO_3_ and KOH_G, the configuration with only one bilayer had similar sensitivity values, ~9 μA cm^{-2} mM^{-1}, the second bilayer lead to a decrease, more significant for the HNO_3_G containing one. For configurations with n = 3 and 4, the sensitivity increases further when chitosan contained KOH_G, to 13.7 and 18.6 μA cm^{-2} mM^{-1}, continuing to decrease for HNO_3_G to 7.0 and 6.0 μA cm^{-2} mM. Deposition of more bilayers did not lead to an increase in sensitivity, probably because of diffusion barriers and due to the resistive nature of chitosan. Moreover, the stability of biosensors based on one and two bilayers was not as good as the one with 4 bilayers, so, taking all this into ac-

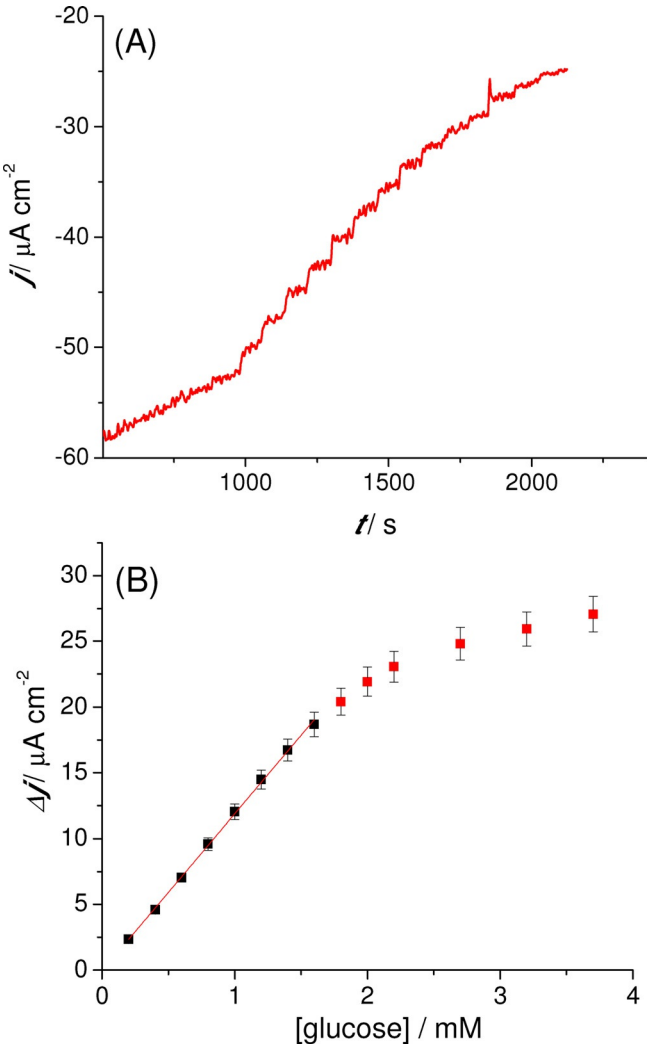

Fig. 5. A) Current vs. time profile recorded in 0.1 M NaPB pH 7.0 at Au/{chit$^+$(KOH_CNT + GOx)/PSS$^-$}$_4$ with successive addition of 0.2 mM glucose and B) corresponding calibration curve; applied potential −0.3 V vs. Ag/AgCl.

Table 3. Analytical parameters of different AuQC/{chit$^+$(CN + GOx)/PSS$^-$}$_4$ biosensors.

CN	Sensitivity (μA cm^{-2} mM^{-1})	*RSD* (n = 3) (%)	*LOD* (μM)
HNO_3_G	6.0 ± 0.3	5.0	64
KOH_G	18.6 ± 0.7	3.8	12
HNO_3_CNT	18.6 ± 0.9	4.8	18
KOH_CNT	13.7 ± 0.7	5.1	50

Table 4. Comparison of analytical parameters of glucose sensors reported in the literature containing comparable electrode materials. PEI: polyethyleneimine; MP11: microperoxidase-11; PAA: polyallylamine; PVS: poly(vinyl sulfate); PDDA: poly(diallyldimethylammonium); SiPy+Cl−: 3-n-propylpyridinium silsesquioxane chloride; CuTsPc: copper(II) tetrasulfophthalocyanine; PPY: polypyrrole; PVI-Os: poly(1-vinylimidazole)–Os complex; PPV: poly(2,5-methoxypropyloxy sulfonatephenylenevinylene); 3DG: 3D graphene; Fc-Chit: ferrocene grafted chitosan hybrid; AuNPs: Au nanoparticles; PV–GNs–NiNPs–Chit: polyvinylpyrrolidone–graphene nanosheets–nickel nanoparticles–chitosan nanocomposite; RGO: reduced graphene oxide; Cu-Co NSs: dendritic copper-cobalt nanostructures.

Biosensor	E (V) vs. Ag AgCl	Sensitivity (μA cm^{-2} mM^{-1})	LOD (μM)	Reference
ITO/(PEI/MP-11)$_2$/(PEI/GOx + liposome)$_1$	+0.1	0.91	8.6	[9]
Au/Thionine/CNT//(PAA/PVS)$_3$/(PDDA/GOx)$_8$	+0.60	19.0	11.0	[15]
GCE/(Thiourea–GOx)$_2$ (0.25 mM Fc)	+0.30	5.73	6.0	[39]
FTO/(SiPy$^+$Cl$^-$/CuTsPc)$_2$(SiPy$^+$Cl$^-$/GOx/Nafion)	–0.10	0.14	160	[40]
ITO/PPY/MWCNT/HRP-GOx ([Fe(CN)$_6$]$^{3-}$)	+0.30	55.2	100	[41]
ITO/PPY/MWCNT/GOx/ ([Fe(CN)$_6$]$^{3-}$)		17.6	300	
SPCE/{PVI-Os/SWCNT/GOx}$_5$	+0.30	16.4	100	[42]
SPCE/{PVI-Os/(SWCNT-GOx)$_{conjugates}$}$_4$	+0.30	32.0	100	[43]
FTO/{PPV/Pt-SiPy$^+$Cl$^-$}$_6$GOx	+0.86	1.2	27.4	[44]
3DG/Fc-Chit/SWCNTs/GOx (not LbL)	+0.4	~60	1.2	[20]
GCE/PVP–GNs–NiNPs–Chit (not LbL)	+0.45	103.8	0.03	[45]
GCE/RGO-Chit/Cu-Co NSs (not LbL)	+0.50	1921	10.0	[46]
AuQC/{chit$^+$(CN + GOx)/PSS$^-$}$_4$	−0.3			This work
CN=KOH_G		18.6	12	
CN=HNO$_3$_CNT		18.6	18	

count, biosensor configurations with 4 layers were considered for comparison and for further evaluation of the biosensors. The variation of sensitivities is similar to the variation of electrode capacitance with the number of bilayers, both being dictated by the dispersion of the carbon nanomaterials in the chitosan layer.

It is worth mentioning that the Au/{chit$^+$(CN + GOx)/PSS$^-$}$_n$ biosensors exhibit very good electrocatalytic performance for glucose detection in terms of the sensitivity and detection limit, similar or superior to those previously reported in the literature based on LbL [9,15,39–44], see Table 4. Just two had higher sensitivities but with higher detection limits [41,43] and two had lower detection limits but much smaller sensitivities [9,39]. As observed in Table 4, all biosensors operate at positive potentials and one of the best advantages of the newly developed biosensors is the negative operating potential, of −0.3 V vs. Ag/AgCl, which allows avoiding all possible electroactive interferents that usually oxidise at positive potentials, such as ascorbate, dopamine, uric acid etc., and demonstrated below in Section 3.5.3. The biosensors which were not constructed by self-assembly, i.e. two non-enzymatic biosensors that contained metal nanoparticles as well as chitosan-graphene [45,46] and one enzymatic one based on a 3D graphene electrode [20] showed better sensitivities, but also had the drawback of operating at positive potentials, which may lead to interferences when used in real matrices, especially in the case of the non-enzymatic ones, due to the lack of the enzymatic selective layer.

A mixture of 0.5% chitosan, 1.0% GOx was also tested in the absence of functionalized G/CNT, the result being a biosensor with very low sensitivity, of 0.73 μA cm^{-2} mM^{-1}, mainly owing to the lack of carbon nanomaterials causing a drastic decrease of the conductivity of the chitosan films, as observed in the CV and EIS evaluation above.

3.5.2 Biosensor Stability

The long-term storage and stability of the modified electrodes was evaluated by measuring the current response for repetitive measurements, testing the biosensors every day during 20 days (excepting weekends), recording an 8-point calibration plot, and results are displayed in Figure 6. All biosensors were stored in NaPB pH 7 at ~4 °C when not in use. The HNO$_3$_CNT biosensors kept more than 90% of the initial sensitivity up to the 10th day; afterwards their sensitivity dropped down to 70% by the 20th day. The same stability profile was observed for the KOH_G biosensors, with the difference that after the 20th day, the sensitivity was 50% of the initial value. The HNO$_3$_G and KOH_CNT biosensors, which had lower initial sensitivities compared to HNO$_3$_CNT and KOH_G, kept 95% of their initial sensitivity up to the 15th day, after which it started to decrease continuously, reaching 60% on the 20th day.

3.5.3 Biosensor Selectivity

The selectivity of the biosensors was determined by the effect of substances which could interfere with glucose measurement, such as ascorbic acid, catechol, citric acid, dopamine, fructose, oxalic acid and uric acid, analyzing their effect on the electrochemical response for 0.3 mM glucose. Ascorbic acid (AA), one of the most important interfering agents in physiological systems, can be eliminated by using negatively charged polymers [47,48], like PSS$^-$, as in the present work. The use of a negative potential, −0.3 V vs. Ag/AgCl is beneficial for eliminating

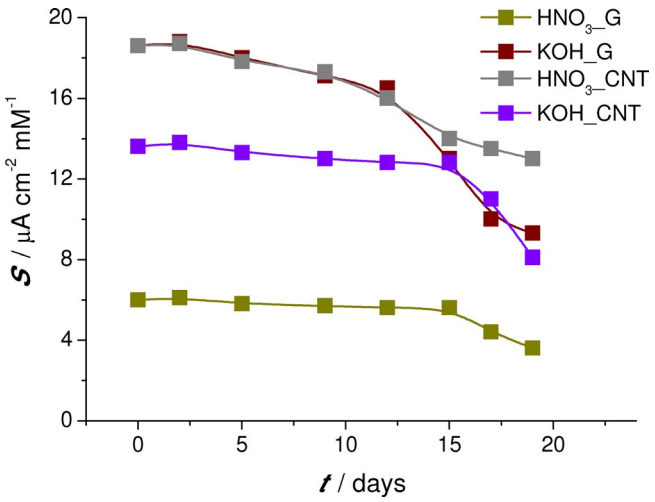

Fig. 6. Sensitivity, *S*, of the Au/{chit$^+$(CN + GOx)/PSS$^-$}$_4$ biosensors over time.

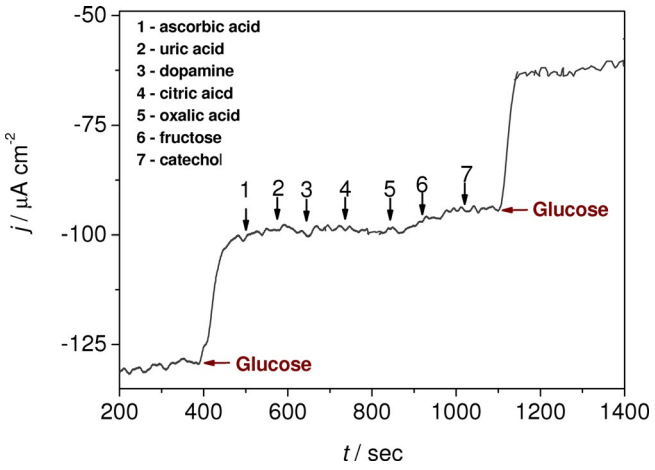

Fig. 7. Current vs. time profile recorded in 0.1 M NaPB pH 7.0 at Au/{chit$^+$(HNO$_3$_CNT + GOx)/PSS$^-$}$_4$ modified electrode with addition of 0.3 mM glucose followed by injection of interferents in a 2 : 1 glucose : interferent concentration ratio.

interferences, since most interferents are electrochemically active at more positive potentials. Figure 7 shows the amperometric response of the biosensor with the addition of 0.3 mM glucose, followed by the injection of all interferent species in a concentration ratio 2 : 1 interferent : glucose. At the end of the measurement procedure, the same concentration of glucose as initially was added, to compare the biosensor response to the enzyme substrate with and without the interfering compounds present in the matrix. As clearly seen in Figure 7, no interferences were found from the compounds tested and, moreover, the biosensor response in their presence was 102.2 ± 0.6 %.

4 Conclusions

Glucose oxidase biosensors, incorporating carbon nanomaterials, functionalised graphene or carbon nanotubes, have been constructed by a layer-by-layer procedure as {chit$^+$(CN + GOx)/PSS$^-$}$_n$. The best GOx biosensors were prepared from enzyme solution containing 0.5 % chitosan and 1 % GOx enzyme incorporating the carbon nanomaterial, the order of sensitivity being in the order HNO$_3$_CNT, KOH_G > KOH_CNT > HNO$_3$_G. This result followed the order of film capacitance values obtained by cyclic voltammetry and electrochemical impedance spectroscopy. The lowest detection limit was 12 µM for the biosensor based on KOH_G. The stability of HNO$_3$_CNT and KOH_G containing biosensors was very good up to the 10th day with more than 90 % of the initial signal. The lack of interferences due to the low working potential required by the present developed biosensors, make them efficient tools for glucose detection in complex matrices.

Acknowledgements

Financial support from *Fundação para a Ciência e a Tecnologia* (*FCT*), *Portugal PTDC/QUI*-QUI/116091/2009, POPH, POCH, POFC-QREN (co-financed by *FSE* and *European Community FEDER funds* through the program COMPETE – Programa Operacional Factores de Competitividade under the projects PEst-C/EME/UI0285/2013 and CENTRO-07-0224-FEDER-002001 (MT4MOBI)) is gratefully acknowledged. M. M.B. thanks *FCT* for a postdoctoral fellowship SFRH/BPD/72656/2010 and M. D. thanks the *European Commission* for a grant under the Erasmus student exchange program BUCURES09. The authors thank Prof. *X. Sun,* University of Western Ontario, Canada for the gift of the graphene.

References

[1] Y. Tan, W. Deng, C. Chen, Q. Xie, L. Lei, Y. Li, Z. Fang, M. Ma, J. Chen, S Yao, *Biosens. Bioelectron.* **2010**, *25*, 2644.
[2] A. Sassolas, L. J. Blum, B. D. Leca-Bouvier, *Biotechnol. Adv.* **2012**, *30*, 489.
[3] M. Campas, B. Bucur, S. Andreescu, J.-L. Marty, *Curr. Top. Biotechnol.* **2004**, *1*, 95.
[4] M. F.M. Choi, *Microchim. Acta* **2004**, *148*, 107.
[5] L. Caseli, D. S. dos Santos Jr., R. F. Aroca, O. N. Oliveira Jr., *Mater. Sci. Eng. C* **2009**, *29*, 1687.
[6] E. M. Pinto, M. M. Barsan, C. M. A. Brett, *J. Phys. Chem. B* **2010**, *114*, 15354.
[7] L. Caseli, David S. dos Santos Jr., M. Foschini, D. Goncalves, Osvaldo N. Oliveira Jr., *Mater. Sci. Eng. C* **2007**, *27*, 1108.
[8] S. Liu, J. Ou, Z. Li, S. Yang, J. Wang, *Appl. Surf. Sci.* **2012**, *258*, 2231.
[9] J. S. Graça, R. F. de Oliveira, M. L. de Moraes, M. Ferreira, *Biochemistry* **2014**, *96*, 37
[10] S. Wu, X. Lan, W. Zhao, Y. Li, L. Zhang, H. Wang, M. Han, S. Tao, *Biosens. Bioelectron.* **2011**, *27*, 82.
[11] Y-C. Yang, S-W. Dong, T. Shen, C-Z. Jian, H-J. Chang, Y. Li, J-X. Zhou, *Electrochim. Acta* **2011**, *56,* 6021.
[12] W. Lian, S. Liu, J. Yu, X. Xing, J. Li, M. Cui, J. Huang, *Biosens. Bioelectron.* **2012**, *38*, 163.

[13] S. A. Miscoria, J. Desbrieres, G. D. Barrera, P. Labbé, G. A. Rivas, *Anal. Chim. Acta* **2006**, *578*, 137.
[14] N. Akbay, J. R. Lakowicz, K. Ray, *J. Phys. Chem. C* **2012**, *116*, 10766.
[15] M. Ma, Z. Miao, D. Zhang, X. Du, Y. Zhang, C. Zhang, J. Lin, Q. Chen, *Biosens. Bioelectron.* **2015**, *64*, 477
[16] M. M. Barsan, M. David, M. Florescu, L. Ţugulea, C. M.A. Brett, *Bioelectrochemistry* **2014**, *99*, 46.
[17] D. Laurent, J. B. Schlenoff, *Langmuir* **1997**, *13*, 1552.
[18] A. K. Sarma, P. Vatsyayan, P. Goswami, S. D. Minteer, *Biosens. Bioelectron.* **2009**, *24*, 2313.
[19] X. Kang, J. Wang, H. Wu, I. A. Aksay, J. Liu, Y. Lin, *Biosens. Bioelectron.* **2009**, *25*, 901.
[20] J Liu, X Wang, T Wang, D Li, F Xi, J Wang, E Wang, *ACS Appl. Mater. Interf.* **2014**, *6*, 19997
[21] Y. Shao, J. Wang, H. Wu, J. Liu, I. A. Aksay, Y. Lin, *Electroanalysis* **2010**, *22*, 1027.
[22] T. Kuila, S. Bose, P. Khanra, A. K. Mishra, N. H. Kim, J. H. Lee, *Biosens. Bioelectron.* **2011**, *26*, 4637.
[23] G. A. Rivas, M. D. Rubianes, M. C. Rodríguez, N. F. Ferreyra, G. L. Luque, M. L. Pedano, S. A. Miscoria, C. Parrado, *Talanta* **2007**, *74*, 291.
[24] G. Wang, L. Zhang, J. Zhang, *Chem. Soc. Rev.* **2012**, *41,* 797.
[25] V. Georgakilas, M. Otyepka, A. B. Bourlinos, V. Chandra, N. Kim, K. C. Kemp, P. Hobza, R. Zboril, K. S. Kim, *Chem. Rev.* **2012**, *112*, 6156.
[26] J. Liu, A. G. Rinzler, H. Dai, J. H. Hafner, R. K. Bradley, P. J. Boul, A. Lu, T. Iverson, K. Shelimov, C. B. Huffman, F. Rodriguez–Macias, Y.-S. Shon, T. R. Lee, D. T. Colbert, R. E. Smalley, *Science* **1998**, *280*, 1253.
[27] T. Ramanathan, F. T. Fisher, R. S. Ruoff, L. C. Brinson, *Chem. Mater.* **2005**, *17*, 1290.
[28] Y. Zhu, S. Murali, M. D. Stoller, K. J. Ganesh, W. Cai, P. J. Ferreira, A. Pirkle, R. M. Wallace, K. A. Cychosz, M. Thommes, D. Su, E. A. Stach, R. S. Ruoff, *Science* **2011**, *332*, 1537.
[29] D. Geng, S. Yang, Y. Zhang, J. Yang, J. Liu, R. Li, T. Sham, X. Sun, S. Ye, S. Knights, *Appl. Surf. Sci.* **2011**, *257*, 9193.
[30] X. Jin, F. Xi, D. Lv, Q. Wu, X. Lin, *Carbohydr. Polym.* **2011**, *85*, 786.
[31] M. M. Barsan, K. P. Prathish, X. Sun, C. M.A. Brett, *Sens. Actuators B* **2014**, *203*, 579–587.
[32] M. M. Barsan, R. C. Carvalho, Y. Zhong, X. Sun, C. M. A. Brett, *Electrochim. Acta* **2012**, *85*, 203–209.
[33] G. Sauerbrey, *Z. Phys.* **1959**, *155*, 206.
[34] H. Luo, Z. Shi, N. Li, Z. Gu, Q. Zhuang, *Anal. Chem.* **2001**, *73*, 915.
[35] X. Lu, J. Hu, X. Yao, Z. Wang, J. Li, *Biomacromolecules* **2006**, *7*, 975.
[36] *Impedance Spectroscopy. Theory Experiment and Applications*, 2nd ed. (Eds: E. Barsoukov, J. R. Macdonald), Wiley, New York, **2005.**
[37] Y.-R. Nian, H. Teng, *J. Electroanal. Chem.* **2003**, *540*, 119.
[38] C. Largeot, C. Portet, J. Chmiola, P.-L. Taberna, Y. Gogotsi, P. Simon, *J. Am. Chem. Soc.* **2008**, *130*, 2730.
[39] A. Salimi, A. Noorbakhsh, *Electrochim. Acta*, **2011**, *17*, 6097.
[40] C. G. de Jesus, D. Lima, V. dos Santos, K. Wohnrath, C. A. Pessôa, *Sens. Actuators B* **2013**, *186*, 44.
[41] K. Singh, B. P. Singh, R. Chauhan, T. Basu, *J. Appl. Polym. Sci.* **2012**, *125*, E235.
[42] Q. Gao, Y. Guo, J. Liu, X. Yuan, H. Qi, C. Zhang, *Bioelectrochemistry* **2011**, *81*, 109. (PVI-Os1)
[43] Q. Gao, Y. Guo, W. Zhang, H. Qi, C. Zhang, *Sens. Actuators B* **2011**, *153*, 219.
[44] V. dos Santos, M. dos Santos, C. G. de Jesus, S. T. Fujiwara, J. R. Garcia, C. A. Pessôa, K. Wohnrath, *Int. J. Electrochem. Sci.* **2013**, *8*, 10601.
[45] Z. Liu, Y. Guo, C. Dong, *Talanta* **2015**, *137*, 87.
[46] L. Wang, Y. Zheng, X. Lu, Z. Li, L. Sun, Y. Song, *Sens. Actuators B* **2014**, *195*, 1.
[47] J. Wang, *Chem. Rev.* **2008**, *108*, 814.
[48] B. K. Jena, C. R. Raj, *Chem. Eur. J.* **2006**, *12*, 2702.

Received: March 16, 2015
Accepted: April 28, 2015
Published online: July 14, 2015

